Separation Science and Technology
Publication details, including instructions for authors and subscription information:
http://www.informaworld.com/smpp/title~content=t713708471

Investigating Characteristics of Increasing Molecular Weight Cutoff Polyamide Nanofiltration Membranes Using Solutes Rejection and Atomic Force Microscopy

A. Wahab Mohammad[a]; Nora'aini Ali[a]; Nidal Hilal[b]
[a] Department of Chemical and Process Engineering, Universiti Kebangsaan Malaysia, UKM Bangi, Selangor Darul Ehsan, Malaysia [b] School of Chemical, Environmental and Mining Engineering, The University of Nottingham, University Park, Nottingham, UK

Online publication date: 19 March 2003

To cite this Article Mohammad, A. Wahab , Ali, Nora'aini and Hilal, Nidal(2003) 'Investigating Characteristics of Increasing Molecular Weight Cutoff Polyamide Nanofiltration Membranes Using Solutes Rejection and Atomic Force Microscopy', Separation Science and Technology, 38: 6, 1307 — 1327
To link to this Article: DOI: 10.1081/SS-120018811
URL: http://dx.doi.org/10.1081/SS-120018811

MARCEL DEKKER, INC. • 270 MADISON AVENUE • NEW YORK, NY 10016

SEPARATION SCIENCE AND TECHNOLOGY
Vol. 38, No. 6, pp. 1307–1327, 2003

Investigating Characteristics of Increasing Molecular Weight Cutoff Polyamide Nanofiltration Membranes Using Solutes Rejection and Atomic Force Microscopy

A. Wahab Mohammad,[1,*] Nora'aini Ali,[1] and Nidal Hilal[2]

[1]Department of Chemical and Process Engineering, Universiti Kebangsaan Malaysia, UKM Bangi, Selangor Darul Ehsan, Malaysia
[2]School of Chemical, Environmental and Mining Engineering, The University of Nottingham, University Park, Nottingham, UK

ABSTRACT

In this article, three nanofiltration (NF) membranes of increasing molecular weight cutoff ranging from 200 to 2000 were characterized by using solute rejection method and atomic force microscope (AFM) imaging. The membranes were all made of polyamide; thus, by using membranes made from the same polymer, it is hoped that the uncertainty imposed by the polymeric materials is eliminated and a better understanding of the relationship between the membrane characteristics and its separation performance is gained. Three approaches were used to fit the solute rejection data: characterization using information provided

*Correspondence: A. Wahab Mohammad, Department of Chemical and Process Engineering, Universiti Kebangsaan Malaysia, 43600 UKM Bangi, Selangor Darul Ehsan, Malaysia; E-mail: wahabm@eng.ukm.my.

DOI: 10.1081/SS-120018811 0149-6395 (Print); 1520-5754 (Online)

MARCEL DEKKER, INC. • 270 MADISON AVENUE • NEW YORK, NY 10016

by the manufacturer, characterization using limiting rejection data, and characterization using the full rejection data. The characterization based on the information by the manufacturer was found to be quite misleading especially for larger pore size membranes. The method based on solute rejection data shows that the characteristics of the membranes were within that expected for NF membranes. It was possible to explain some of the membrane rejection performance based on the characteristics obtained. However, the result from AFM study shows the existence of wide pore size distribution of the membranes. This may be the reason why there have been some inconsistencies and non-uniformity in the membranes performance.

Key Words: Nanofiltration; Atomic force microscopy; Characterization; Pore radius; Charge density.

INTRODUCTION

Nanofiltration (NF) membranes have been recognized for having properties in between those of ultrafiltration (UF) and reverse osmosis (RO) and thus have found applications in many areas especially in rejecting ions and charged organic pollutants. Due to the charged (mostly negative) nature of the membranes, the separation performance is influenced not only by the steric effect but also the charge or Donnan effect. In trying to model the performance of NF membranes, the membranes are typically characterized in terms of the effective pore radius, r_p, (accounting for steric effect) and effective charge density, X_d, (for Donnan effect).[1–7] An additional parameter would normally be the effective ratio of membrane thickness over porosity, $\Delta x/A_k$. Once these parameters are obtained, it is possible to use models such as those based on the extended Nernst–Planck equation to simulate the separation performance of the membranes.[8]

Various studies have been carried out to quantify the above three parameters. For r_p and $\Delta x/A_k$, the most commonly used method is by interpreting the solute rejection of various uncharged solutes by using a hydrodynamic or pore model, which describes the diffusive and convective transport of spherical solutes through the membranes.[3–7] A more direct approach to measure r_p is by visually imaging the membrane surface using the atomic force microscope.[7,9] Similarly X_d has been quantified by using rejection of salts such as NaCl in conjunction with model based on the extended Nernst–Planck equation. Other methods to measure the charge properties of NF membranes include streaming potential measurements, titration and membrane potential measurement.[2]

One of the weaknesses of the previous characterization works, however, have been due to the fact that membranes of different polymer types were characterized and comparison was made on their properties.[1–4] In such cases, it is difficult to make proper comparison and conclusion based on the findings because different polymers may cause different additional effects on the membrane characteristics. The interplay between steric and Donnan effects have been shown theoretically by Bowen and Mohammad[10] to have impacts on the optimum separation performance as well as operating conditions for NF operations. Thus, it is quite imperative to study the variations of the steric and Donnan properties of NF membranes made from the same material.

In this study, we planned to investigate the characteristics of three commercially available polyamide NF membranes with reported molecular weight cutoff (MWCO) ranging from 200 to 2000. The membranes were first characterized by using solute (salt and neutral solutes) rejections in conjunction with available mathematical models to obtain estimate of the effective pore radius, r_p, effective charge density, X_d, and the effective ratio of membrane thickness over porosity, $\Delta x/A_k$. All three membranes were then subjected to surface imaging by using atomic force microscope to further confirm the pore dimension. By using NF membrane made from the same polymer, we hope to eliminate the uncertainty imposed by the polymeric materials and thus obtain a better understanding of the relationship between the three membrane parameters and their separation performance.

CHARACTERIZATION METHODS

Methods Using Solute Rejections

For uncharged solutes, the hydrodynamic model for transport of solute across the membrane considers only the diffusive and convective flows. The solute flux can thus, be expressed as

$$j_i = -D_{i,p}\frac{dc_i}{dx} + K_{i,c}c_iV \tag{1}$$

The hindered nature of diffusion and convection of the ions inside the membrane are accounted for by the terms $K_{i,d}$ and $K_{i,c}$, which are related to the hydrodynamic coefficients, K^{-1}, the enhanced drag, and G, the lag

coefficient of a spherical solute moving inside a cylindrical pore of infinite length. Bowen et al.[7] suggested the use of the following equations,

$$K_{i,d} = K^{-1}(\lambda, 0) \quad \text{where}$$

$$K^{-1}(\lambda, 0) = 1.0 - 2.30\lambda + 1.154\lambda^2 + 0.224\lambda^3 \tag{2}$$

$$K_{i,c} = (2 - \Phi)G(\lambda, 0) \quad \text{where}$$

$$G(\lambda, 0) = 1.0 + 0.054\lambda - 0.988\lambda^2 + 0.441\lambda^3 \tag{3}$$

To obtain an expression for rejection of the solute, Eq. (1) is integrated across the membrane with the solute concentrations in the membrane at the upper ($x = 0$) and lower ($x = \Delta x$) surfaces expressed in terms of the external concentrations ($C_{i,m}$ and $C_{i,p}$) using the equilibrium partition coefficient, Φ,

$$\Phi = \frac{c_{i,x=0}}{C_{i,w}} = \frac{c_{i,x=\Delta x}}{C_{i,p}} = \left(1 - \frac{r_s}{r_p}\right)^2 \tag{4}$$

Equation (1) can be integrated and combined with Eq. (4) to give the following expression for calculated real rejection,

$$R_{real} = 1 - \frac{K_{i,c}\Phi}{1 - \exp(-Pe_m)[1 - \Phi K_{i,c}]} \tag{5}$$

where the Peclet number, Pe_m, is defined as

$$Pe_m = \frac{K_{i,c}}{K_{i,d}} \frac{V\Delta x}{D_{i,\infty}A_k} \tag{6}$$

In the limiting case of the $Pe_m \rightarrow \infty$, the asymptotic rejection values will go to

$$R_{lim} = 1 - \Phi K_{i,c} \tag{7}$$

Thus, $(1 - \Phi K_{i,c})$ represents a parameter for comparing the limiting rejections of solutes of various sizes. The Hagen–Poiseuille equation relates the water flux to the applied pressure as well as r_p and $\Delta x/A_k$.

$$J_w = \frac{r_p^2 \Delta P}{8\mu(\Delta x/A_k)} \tag{8}$$

The membrane parameters r_p and $\Delta x/A_k$ can be determined by fitting the solute rejection data as a function of flux to Eq. (5).

For charged solutes such as salts, the extended Nernst–Planck equation forms the basis for the description of the transport of ions/solutes inside the membranes. The equation can be written as

$$j_i = -D_{i,p}\frac{dc_i}{dx} - \frac{z_i c_i D_{i,p}}{RT} F \frac{d\psi}{dx} + K_{i,c} c_i V \tag{9}$$

where j_i is the flux of ion i and the terms on the right hand side represent transport due to diffusion, electric field gradient, and convection, respectively. Further details for solution of this equation for transport through NF membranes can be found elsewhere.[5,7]

After obtaining the effective pore radius, r_p, and effective ratio of membrane thickness to porosity, $\Delta x/A_k$, by fitting the uncharged solute rejection data, the effective charge density, X_d, can be determined by fitting the rejection data of NaCl to the extended Nernst–Planck model.

Approximate Characterization Method Using Manufacturer's Data

Bowen and Mohammad[5] proposed an approximate characterization method, which uses specification data obtained from the membrane manufacturers to determine the structural parameters such as r_p, $\Delta x/A_k$, and X_d. The information is normally given in terms of very limited membrane permeability at high salt rejection. Table 1 shows the information given by the manufacturer for the three membranes used in this study. Given such information, the value of r_p can be approximated by assuming that the rejection provided is the limiting rejection and Eq. (3) is used with assumption of $Pe_m \rightarrow \infty$, the Hagen–Poiseuille Eq. (5) will then allow us to determine $\Delta x/A_k$.

For data given in MWCO, it was assumed that the given molecular weight corresponds to a 90% rejection of solute. Thus, R_{lim} will be equal to 0.9. For the hypothetical molecule with the respective MWCO,

Table 1. Information on the membrane as provided by the manufacturer.

Membrane	Material	Molecular weight cutoff (Dalton)	P_{max} (bar)	T_{max} (°C)	Water flux ($l\,m^{-2}\,h^{-1}$)
BM02/D	Polyamide	200	30	50	200
BM05/D	Polyamide	500	25	50	300
BM20/D	Polyamide	2000	15	50	310

the following equation correlates the radius of the hypothetical solute at a given MW and r_s.[5]

$$\log_{10} r_s = -1.3363 + 0.395 \log_{10} M_w \quad (10)$$

Method Using Atomic Force Microscope

Atomic force microscopy (AFM)[11] is a relatively newly developed technique that gives topographic images by scanning a sharp tip over a surface[12] and has been used to produce atomic resolution images of both conductors and non-conductors.[13] AFM can image non-conducting surfaces with nanometer-scale resolution in air and even under liquids. Consequently, the samples need not be exposed to vacuum and preparation techniques such as evaporating a thin metal coating or taking a replica. Even soft organic surfaces can be successfully imaged with AFM because the use of microfabricated cantilevers[13] allows operation with total forces between 10^{-7} and 10^{-8} N in contact mode and in the order of 10^{-12} N in non-contact mode.

The study of the surface morphology of membranes can help to understand the separation processes in these membranes as the characteristics of pore structure (pore diameter, pore density, and pore size distribution) determine their filtration properties. However, a high-resolution microscope is necessary to observe the small pores especially in nanofiltration membranes.[7,14,15]

AFM has also been used to elucidate the mechanisms giving rise to inefficiencies (fouling) in membrane processing.[16] However, most studies on membranes have been studied in "contact mode." In this mode, also known as repulsive mode, the tip is very close ("in contact") to the surface being imaged and is responding to very short-range repulsive interactions with the sample. In a second mode of operation, "non-contact mode," the tip instead responds to attractive van der Waals interactions with the sample. These are longer range, so the tip is generally at a distance of 5–10 nm away from the surface while imaging. This mode of operation is especially suitable for polymeric membranes as reported previously.[14,17,18]

The present article reports a study of the use of non-contact AFM to investigate the surface pore structure of three types of nanofiltration membranes: BM20/D, BM05/D, and BM02/D. Quantitative measurements of pore size and pore size distribution have been obtained. The results show that

non-contact AFM is an excellent means of obtaining such information for nanofiltration membranes.

METHODOLOGY

Membranes

Flat sheet samples of three commercial NF membranes, BM02/D, BM05/D, and BM 20/D with MWCO 200, 500, and 2000, respectively, produced by Berghoff Filtration, Germany were used. They are negatively charged membranes made of polyamide. To eliminate any compression effects, each membrane was pressurized at 10 bars for at least 2 hr.

Permeation Experiment

Glucose (MW = 180), maltose (MW = 342), and vitamin B12 (MW = 1355) were chosen as neutral solutes, and NaCl was used as the charged solute. The neutral solutes concentrations were measured with UV spectrophotometer while the salt concentration was analyzed by using a conductivity meter. For the saccharide solutions, they were treated with DNS reagent using DNS method prior to UV spectrophotometers.[19] The concentration of vitamin B12 used was 100 mg/L, whereas that for glucose and maltose was 500 mg/L. The concentration of NaCl used ranged from 1 to 100 mol/m^3. Solution pH in all cases was neutral in the range of 6.5–6.7 while the temperature was maintained at 25 ± 0.5°C. Table 2 shows the diffusivity and solute radius and of each ion and solute.

An Osmonics SEPA ST Stirred Cell was used in the permeation experiments. It has a volume capacity of 300 mL and can hold a membrane

Table 2. Characteristics of ions and solutes in the study.

Ions or solutes	$D_{i,\infty} \times 10^9 (m^2 s^{-1})$	$r_i \times 10^{10}$ (m)
Na^+	1.33	1.84
Cl^-	2.03	1.21
Glucose	0.69	3.60
Maltose	0.52	4.70
Vitamin B12	0.33	7.40

disc of 49 mm in diameter. The effective area of the membrane is 16.9 cm^2. The maximum operating pressure of the cell is 450 psig. First, experiments were carried out with distilled water. For each type of membrane, three samples were used in this study, and the average water permeate values were reported. The pure water flux J_v was measured at different transmembrane pressures to determine the water permeability, P_m from $J_v = P_m \Delta P$. For each sample, the pressure was first increased and then decreased, with good reproducibility. Then, experiments were carried out with the solutes.

The stirring speed was fixed at 400 rpm and range of operating pressures of 2 bars to 26 bars to obtain flux range between 0 and 8×10^{-6} m/sec. For each operating condition, the flux and observed rejection were determined accordingly. The real rejection was determined by using the following definition of wall concentration, C_w:

$$C_w = \exp(J_v/k)(C_b - C_p) + C_p \tag{11}$$

where the mass transfer coefficient is calculated through the following correlations[7]

$$k = 0.23\left(\frac{r^2}{\upsilon}\right)^{0.567}\left(\frac{\upsilon}{D_{\text{eff},\infty}}\right)^{0.33}\frac{D_{\text{eff},\infty}}{r}\omega^{0.567} \tag{12}$$

The real rejection is given by,

$$R_{\text{real}} = 1 - \frac{C_p}{C_w} \tag{13}$$

Method Using Atomic Force Microscope

The AFM used in the present study was a commercial device from Vecco Instruments (USA). High-magnification images of membrane surfaces can be obtained with the use of microfabricated cantilevers.[20] In the present work, Ultralevers (Park Scientific Instruments) were used. These are silicon cantilevers with a high aspect ratio tip of typical radius of curvature ~ 10 nm. Non-contact AFM measures long-range attractive van der Waals forces between the tip and the sample; the tip is held about 5–10 nm above the sample surface during the scan. Because these forces are much weaker than the repulsive forces measured in contact mode, a highly sensitive modulation technique is used to detect the small force gradients. A stiff cantilever is vibrated near its resonance frequency (typically 100–400 kHz) with amplitude of a few nanometers, and changes in the cantilever resonance are detected

MARCEL DEKKER, INC. • 270 MADISON AVENUE • NEW YORK, NY 10016

as the tip is scanned above the sample surface. While scanning the sharp tip above the surface, the vertical motion of the tip due to interatomic forces, is detected by sensing, with a two-segment photodiode, the deflection of a laser beam reflected off the back of the cantilever. In operation, the sample is moved under the tip while a z-feedback loop operates to maintain a constant force on the cantilever tip (a constant vibration amplitude) by adjusting the tip-to-sample spacing. The z voltage applied to the (piezoelectric) scanner to maintain constant attractive force is used to map out the surface topography. A scan rate of 1 Hz was used with 256×256 pixel resolution for the three investigated nanofiltration membranes.

RESULT AND DISCUSSION

Water Flux Measurement

The permeability of each type of membrane was determined by the measurement of water flux as a function of applied pressure. For each membrane, fluxes for three membrane samples were measured. The average flux for the three membranes is shown in Fig. 1 together with the standard deviation. In all cases, the water flux was a linear function of the applied pressure, $J_v = P_m \Delta P$. The deviation from average value of permeability coefficient for all three samples of membrane BM20/D, BM05/D, and BM02/D varied between 14 and 28%, 4 and 20%, and 3 and 7%, respectively. The permeability of the membranes increased in the sequence BM02/D $<$ BM05/D $<$ BM20/D. As shown in Fig. 1, the standard deviations for the three membrane samples, especially for BM20/D and BM05/D, were quite large. It is postulated that the pores of the membranes were quite non-uniform, and thus the membrane possibly have very wide pore size distribution. The use of AFM in subsequent work should be able to verify this assumption.

Characterization Using Uncharged Solutes and Salts

In characterizing the membranes by using uncharged solutes and salts, three approaches were used to fit the rejection data. The three approaches are: (1) characterization using information provided by the manufacturer, (2) characterization using limiting rejection data, and (3) characterization using the full rejection data. These three approaches were described in the previous section. The main reason in using the three approaches is to compare the effectiveness of the three approaches in providing acceptable

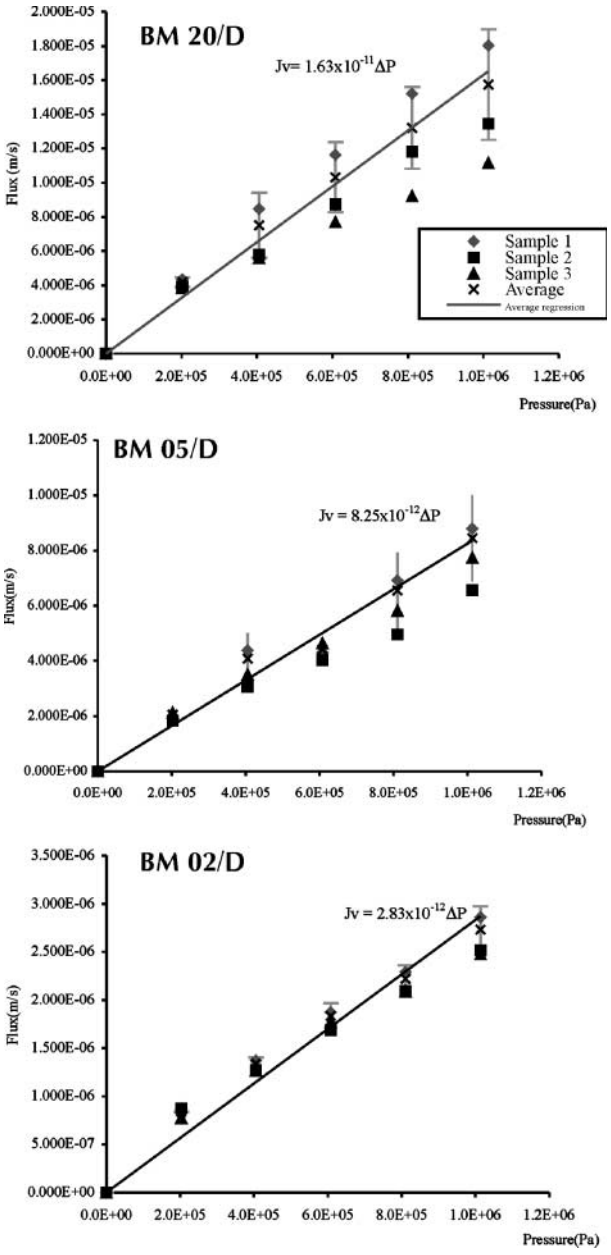

Figure 1. Water flux measurement as a function of pressure.

characterization parameters of the membranes. In addition, it was found that all the rejection data approached the limiting value and thus justifying the use of the second approach. The uncharged solutes used were glucose, maltose, and vitamin B12. The solutes have a very similar structure and polarity, and as shown in Table 2, the Stokes radius ranges from 0.34 to 0.8 nm, which covered the whole spectrum of pore size distribution in the membranes.

Figure 2 shows the real rejection, R_{real} of neutral solutes vs. flux. The R_{real} was found to increase only slightly as the flux increased and approaching toward a limiting value, R_{lim}. For each membrane, the highest rejection is shown by vitamin B12, followed by maltose and glucose. The rejection pattern of the membranes showed a tendency to reach the limiting rejection even at low flux (around $2\,m^3\,m^{-2}\,s^{-1}$).

The first approach used only the manufacturer's data on MWCO and water flux to estimate the pore radius, r_p and effective thickness over porosity, $\Delta x/A_k$. The MWCO was assumed to correspond to 90% rejection of a hypothetical solute with the respective molecular weight. Equation (10) was then used to estimate the radius of the hypothetical solute. Thus, based on the limiting rejection of the solute approaching 90%, the r_p can be estimated from Eq. (7). In the second approach, the limiting rejections of vitamin B12, maltose, and glucose were estimated based on the experimental data shown in Fig. 2. Again Eq. (7) was used to estimate the pore radius, r_p, for all the three solutes. In both cases, once the r_p was obtained, the Hagen–Poiseuille Eq. (8) was used to obtain $\Delta x/A_k$. In the third approach,

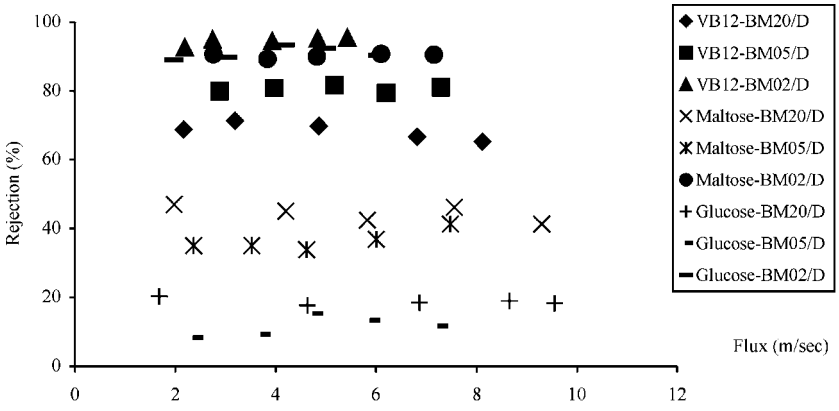

Figure 2. Rejection plot of neutral solutes.

Table 3. The value of structural parameters for the membranes obtained from the three approaches.

Membrane	Method	r_p[a](nm)	$\Delta x/A_k$[a] (μm)
BM20/D	Approximate characterization	1.19	13.38
	Limiting rejection	1.17	12.83
	Full-range rejection	1.28	98.88
BM05/D	Approximate characterization	0.69	8.80
	Limiting rejection	1.21	27.23
	Full-range rejection	1.11	77.98
BM02/D	Approximate characterization	0.48	12.40
	Limiting rejection	0.64	23.54
	Full-range rejection	0.52	91.5

[a] Average obtained from data of the three solutes used.

the rejection data of vitamin B12, maltose, and glucose were fitted to Eq. (6) to obtain independently r_p and $\Delta x/A_k$.

Table 3 shows the value obtained for r_p and $\Delta x/A_k$ from the three above-mentioned approaches. Based on Table 3, it was shown that in general the r_p obtained from the three approaches were within 20% of each other except for membrane BM05/D. For this membrane, the MWCO provided by the manufacturer was quite deviated from the membrane performance. Thus r_p based on the MWCO data was estimated to be much lower compared to those obtained using the experimental data. The BM05/D and BM20/D were found to have similar rejections of the uncharged solutes and thus the estimated r_p's were quite similar. The lower flux performance for membrane BM05/D was due to higher effective thickness over porosity ratio.

Characterization Using Salt Rejection Data

Permeation experiments were carried out with NaCl solution. Figure 3 shows the rejection plot of NaCl with three different membrane as a function of the permeate flux. Bulk concentration used was fixed at $10\,\mathrm{mol\,m^{-3}}$. Rejection pattern was the same as the rejection of neutral solute. The rejection data were then used to fit the effective charge density, X_d, values using the Donnan-Steric-Pore model. Because the manufacturer did not provide any salt rejection data, it was not possible to use the structural parameters, r_p and $\Delta x/A_k$, from the first approach to determine X_d. The data were then fitted by

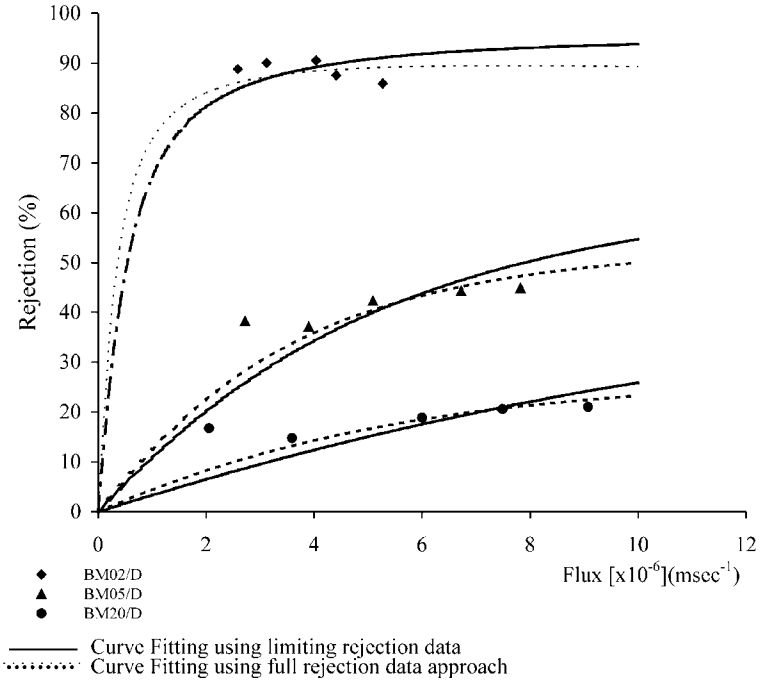

Figure 3. Rejection of sodium chloride solution for the three membranes.

using r_p and $\Delta x/A_k$ obtained from the second and third approaches. Table 4 shows the X_d values obtained from model fittings. The third column in Table 4 shows the ratio of effective charge density over bulk concentration, X_d/C_b. The values obtained for this study were within the range of reported values for commercially available NF membranes reported previously.[5]

Table 4. X_d values for three different membranes.

Membrane	Method	X_d (mol m^{-3})	X_d/C_b
BM20/D	Limiting rejection	64.9	6.49
	Full-range rejection	22.7	2.27
BM05/D	Limiting rejection	97.1	9.71
	Full-range rejection	46.3	4.63
BM02/D	Limiting rejection	509.0	50.9
	Full-range rejection	136.1	13.6

As shown in Fig. 3, the data were fitted well with both set of values obtained from the two approaches. However, the X_d calculated by using the parameters from the second approach (based on limiting rejection) was found to be much higher than that obtained by using the parameters from the third approach.

Based on the fitted parameters of r_p and X_d, the rejection mechanism of the three membranes can be explained. For the three membranes, the rejection follows the sequence: BM02/D > BM05/D > BM20/D. Membrane BM02/D showed consistently high rejection: almost 90% rejection. This is due to the combination of small pore size (≈ 0.5 nm) and large X_d that caused the chloride ions to be rejected by the membranes. For BM05/D and BM20/D, even though the difference in r_p is rather small, the rejection of BM05/D was almost double the BM20/D rejection (0–44% for BM05/D, 0–28% for BM20/D). This may be due to the higher effective charge inherent in BM05/D membrane.

The results thus far have shown that the membrane characteristics can be quite varied in terms of the r_p, X_d, and $\Delta x/A_k$. Bowen and Mohammad[9] proposed the use of optimized membrane parameters, i.e., NF membranes with selected properties such that these properties are unique to the separation of interest. The ability to produce NF membranes with optimized characteristics will certainly help to reduce the cost as well as improving processing time for membrane processes. The result from this study showed that there is a potential for developing NF membranes with varying properties of r_p, X_d, and $\Delta x/A_k$.

Characterization Using Atomic Force Microscope

It should be noted that the pore dimension obtained using AFM is not exact due to the uncertainty in absolute dimension measurements caused by convolution of the AFM tip and pore shapes at the nanometer scale.[21] Thus, the result from AFM will be used for relative comparison of the pore dimension as well as to determine the pore size distribution of the membranes.

As shown in Fig. 4, the AFM images of the three membranes clearly show the presence of pores in the membranes. A tighter structure is clearly displayed for membrane BM02/D, whereas the loosest structure is for membrane BM20/D. The following equation was used to fit the pore size distribution[22]:

$$f = f_{\max} e^{[-1/(2\sigma^2)](\ln(r_p/\mu))^2} \tag{21}$$

MARCEL DEKKER, INC. • 270 MADISON AVENUE • NEW YORK, NY 10016

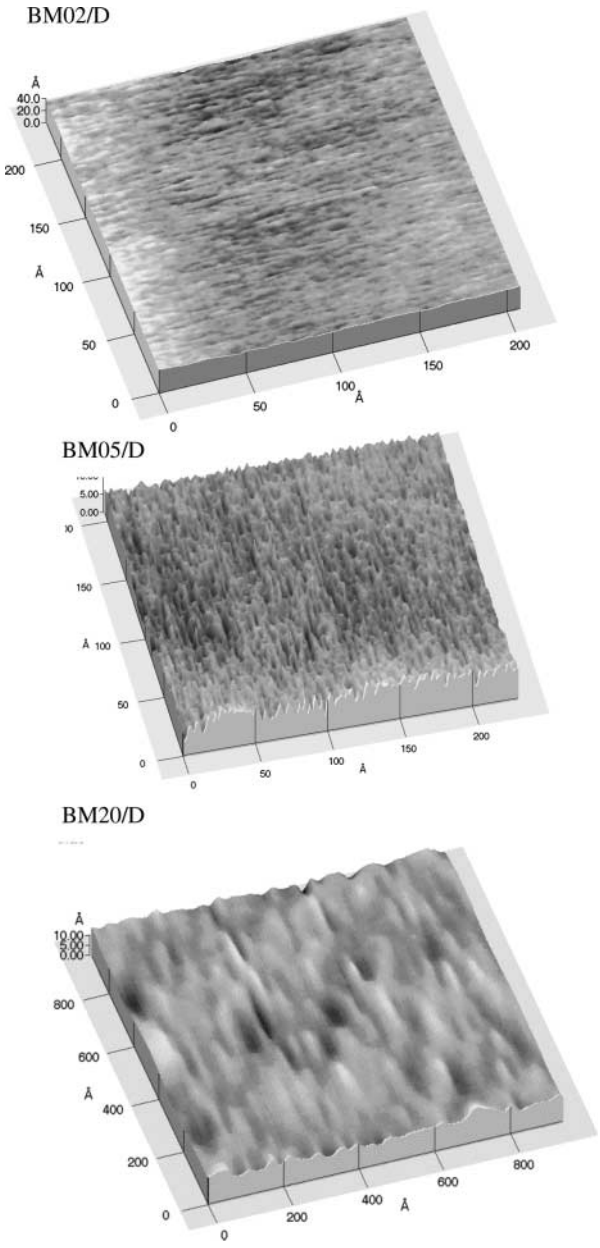

Figure 4. AFM image of the three membranes.

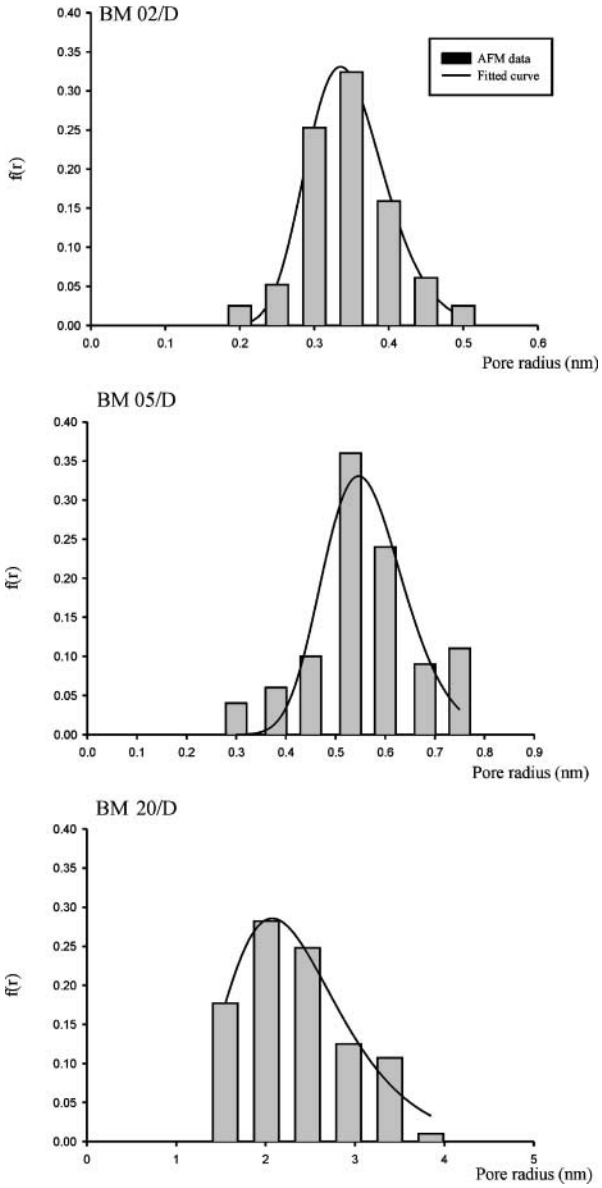

Figure 5. Pore size distribution for the three membranes.

Table 5. Values of constants obtained from fitted curves (log normal distribution) for BM02/D, BM05/D, and BM20/D.

Membrane ID	R square	a (maximum of f)	μ (nm) (most probable r_p)	σ (nm) (standard deviation)
BM20/D	0.956	0.286 ± 0.022	2.075 ± 0.059	0.30 ± 0.03
BM05/D	0.829	0.331 ± 0.050	0.546 ± 0.015	0.15 ± 0.03
BM02/D	0.988	0.331 ± 0.014	0.351 ± 0.003	0.15 ± 0.01

where f is the density of pore, f_{max} is the maximum of f, μ is the value of r_p that makes f maximum (most probable r_p), and σ is the standard deviation or width of the distribution. Figure 5 shows that the pore size distribution obtained from AFM for all membranes were fitted well with Eq. (21). Table 5 shows the values of mean pore radius and its standard deviation, obtained from fitted curves for all membranes. The theoretical distribution is well fitted with the experimental data, providing a good justification for the use of such a distribution in calculations. The estimated r_p from the AFM image were much lower for BM02/D and BM05/D compared to those obtained by using solute rejection. For BM20/D, however, the r_p was unexpectedly much larger than that estimated from solute rejection. For BM20/D also, the standard deviation, σ is quite large compared with the other two membranes. The large standard deviation may explain the large variation in water flux measurement for BM20/D membrane. The discrepancies between the AFM measurements and solute rejection data were also observed by other researchers previously.[21,23]

In interpreting the results obtained in this study, one should be careful with regard to the effect of pore size distribution of the membranes. The solute rejection models assumed only an absolute effective pore radius in describing the transport mechanism. In actuality, as shown by the result from AFM, the pore size distribution of the membranes can be quite wide. This may be the reason why there has been some non-uniformity in the membrane performance from different samples. A more sophisticated model, which takes into account the effect of pore size distribution in the solute transport, such as that proposed recently by Bowen and Welfoot,[4] may be able to further elucidate the discrepancies observed in this study.

CONCLUSION

In this study, we characterize three NF membranes of increasing molecular weight cutoff ranging from 200 to 2000 using solute rejection

method and atomic force microscope imaging. The membranes were all made of polyamide and thus by using membranes made from the same polymer, we hope to eliminate the uncertainty imposed by the polymeric materials and thus obtain a better understanding of the relationship between the three membrane parameters and their separation performance. Three approaches were used to fit the solute rejection data: characterization using information provided by the manufacturer, characterization using limiting rejection data, and characterization using the full rejection data. The characterization based on the information by the manufacturer was found to be quite misleading especially for larger pore size membranes. The method based on solute rejection data shows that the characteristics of the membranes were within that expected for NF membranes. It was possible to explain some of the membrane rejection performance based on the characteristics obtained. However, the result from AFM study shows the existence of wide pore size distribution of the membranes. This may be the reason why there have been some inconsistencies and non-uniformity in the membranes' performance.

NOMENCLATURE

A_k	porosity
c_i	concentration in membrane ($mol\,m^{-3}$)
$C_{i,b}$	concentration in the bulk solution ($mol\,m^{-3}$)
$C_{i,p}$	concentration in permeate ($mol\,m^{-3}$)
$D_{eff,\infty}$	effective bulk diffusivity ($m^2\,s^{-1}$)
$D_{i,p}$	hindered diffusivity ($m^2\,s^{-1}$)
$D_{i,\infty}$	bulk diffusivity ($m^2\,s^{-1}$)
F	Faraday constant ($C\,mol^{-1}$)
G	enhanced drag coefficient
j_i	ion flux (based on membrane area) ($mol\,m^{-2}\,s^{-1}$)
k	mass transfer coefficient
$K_{i,c}$	hindrance factor for convection
K^{-1}	hydrodynamic coefficient
$K_{i,d}$	hindrance factor for diffusion
Pe_m	Peclet number
P_m	permeability constant ($m^3\,m^{-2}\,s^{-1}\,Pa^{-1}$)
ΔP	applied pressure drop (bar)
r_p	effective pore radius (m)
r_s	solute radius (m)
R	gas constant ($J\,mol^{-1}\,K^{-1}$)

R_{real}	real rejection
R_{lim}	limiting real rejection
T	absolute temperature (K)
x	distance normal to membrane (m)
Δx	effective membrane thickness (m)
X_d	effective membrane charge (mol m^{-3})
z_i	valence of ion
λ	ratio of solute radius to pore radius
Φ	steric partitioning coefficient
δ	thickness of film layer (m)
$\Delta\psi$	potential difference (V)
υ	kinematic viscosity ($m^2\,s^{-1}$)
ω	stirring speed (rad s^{-1})

ACKNOWLEDGMENT

The authors thank the Malaysian Ministry of Science, Technology & Environment for sponsoring the work under project IRPA 09-02-02-0067.

REFERENCES

1. Wang, X.L.; Tsuru, T.; Togoh, M.; Nakao, S.; Kimura, S. The electrostatic and steric-hindrance model for the transport of charged solutes through nanofiltration membrane. J. Membr. Sci. **1997**, *135*, 19–32.
2. Schaep, J.; Vandecasteele, C. Evaluating the charge of nanofiltration membranes. J. Membr. Sci. **2001**, *188*, 129–136.
3. Schaep, J.; Vandecasteele, C.; Mohammad, A.W.; Bowen, W.R. Modelling the retention of ionic components for different membrane. Sep. Purif. Technol. **2001**, *22–23* (1–3), 169–179.
4. Bowen, W.R.; Welfoot, J.S. Modelling the performance of membrane nanofiltration—critical assessment and model development. Chem. Eng. Sci. **2002**, *57* (8), 1393–1407.
5. Bowen, W.R.; Mohammad, A.W. Characterization and prediction of nanofiltration membrane performance—a general assessment. Trans. IChemE **1998**, *76A*, 885–893.
6. Schaep, J.; Vandecasteele, C.; Mohammad, A.W.; Bowen, W.R. Analysis of the salt retention of nanofiltration membrane using the Donnan-steric partitioning pore model. Sep. Sci. Technol. **1999**, *34* (15), 3009–3030.

7. Bowen, W.R.; Mohammad, A.W.; Hilal, N. Characterization of nanofiltration membrane for predictive purposes—use of salts, uncharged solutes and atomic force microscopy. J. Membr. Sci. **1997**, *126*, 91–905.
8. Mohammad, A.W. A modified Donnan-steric-pore model for predicting flux and rejection of dye/NaCl mixture in nanofiltration membranes. Sep. Sci. Technol. **2002**, *37* (5), 1009–1030.
9. Bowen, W.R.; Doneva, T. AFM studies of nanofiltration membrane: surface morphology, pore size distribution and adhesion. Desalination **2000**, *117*, 163–172.
10. Bowen, W.R.; Mohammad, A.W. A theoretical basis for specifying nanofiltration membrane—dye/salt/water stream. Desalination **1998**, *117*, 257–264.
11. Binning, G.; Quate, C.F.; Gerber, Ch. Atomic force microscope. Phys. Rev. Lett. **1986**, *56*, 930–933.
12. Hansma, P.K.; Elings, V.B.; Marti, O.; Bracker, C.E. Scanning tunnelling microscopy and atomic force microscopy: applications to biology and technology. Science **1988**, *242*, 209–216.
13. Albrecht, T.R.; Quate, C.F. Atomic resolution with the atomic force microscope on conductors and non-conductors. J. Vac. Sci. Technol. A **1988**, *6*, 271–275.
14. Bowen, W.R.; Hilal, N.; Lovitt, R.W.; Wright, C.J. Atomic force microscope studies of membrane surfaces. In *Surface Chemistry and Electrochemistry of Membrane Surfaces-Volume 79*; Sørensen, T.S., Ed.; Surfactant Science Series; Marcel Dekker Inc: USA, 1999; Chap. 1, 1–37.
15. Bowen, W.R.; Hilal, N.; Jain, M.; Lovitt, R.W.; Mohammad, A.W.; Sharif, A.O.; Williams, P.M.; Wright, C.J. Ab initio prediction of the performance of membrane separation processes. In *Comprehensive Chemical Kinetics, Volume 37—Application of Kinetic Modelling*; Compton, R.G., Hancock, G., Eds.; Elsevier Science B. V., 1999; 524–541.
16. Bowen, W.R.; Hilal, N.; Lovitt, R.W.; Wright, C.J. A new technique for membrane characterisation: direct measurement of the force of adhesion of a single particle using an atomic force microscope. J. Membr. Sci. **1998**, *139*, 269–274.
17. Bowen, W.R.; Hilal, N.; Lovitt, R.W.; Williams, P.M. Visualisation of an ultrafiltration membrane by non-contact atomic force microscopy at single pore resolution. J. Membr. Sci. **1996**, *110* (2), 229–232.
18. Bowen, W.R.; Hilal, N.; Lovitt, R.W.; Williams, P.M. Atomic force microscope studies of membranes: surface pore structures of anopore and cyclopore membranes. J. Membr. Sci. **1996**, *110* (2), 233–238.

19. Miller, G.L. Use of dinitrosalicylic acid reagent for the determination of reducing sugars. Anal. Chem. **1969**, *3*, 426–428.
20. Sarid, D. *Scanning Force Microscopy*; Oxford University Press, 1994.
21. Bowen, W.R.; Welfoot, J.S. Modelling of membrane nanofiltration—pore size distribution effects. Chem. Eng. Sci. **2002**, *57* (8), 1393–1407.
22. Ochoa, N.A.; Pradanos, P.; Palacio, L.; Pagliero, C.; Marchese, J.; Hernandez, A. Pore size distributions based on AFM imaging and retention of multidisperse polymer solutes characterization of polyethersulfone UF membranes with dopes containing different PVP. J. Membr. Sci. **2001**, *187*, 227–237.
23. Singh, S.; Khulbe, K.C.; Matsuura, T.; Ramamurthy, P. Membrane characterization by solute transport and atomic force microscopy. J. Membr. Sci. **1998**, *142*, 111–127.

Received July 2002
Revised October 2002